

Numerical Modelling Of The Fire Behaviour Of Reinforced Concrete Beam Integrating The Concrete Cover Lost By Spalling

Cherif GUERGAH^{*1}, Mohamed Salah² DIMIA and Mohamed GUENFOUD³

^{*1}Laboratory of Civil Engineering and Hydraulics, University of Guelma, Algeria

²Department of civil Engineering, University of Batna, Algeria

³Laboratory of Civil Engineering and Hydraulics, University of Guelma, Algeria

Received 29 Sep 2016,
Revised 26 Apr 2017,
Accepted 29 Apr 2017

Keywords

- ✓ Fire;
- ✓ Spalling;
- ✓ Beam;
- ✓ Reinforced concrete;
- ✓ Modelling;
- ✓ SAFIR

Guergah Cherif
guergah.cherif@yahoo.fr

Abstract

The aim of the paper is the realization of a numerical study, in which the concrete spalling phenomenon of structural elements (beams) in reinforced concrete subject to hydrocarbon fire (HC) is considered, and its influence on structural stability is analyzed. The manifestation of this phenomenon can start during the first few minutes, exposing the reinforcement nearest to the fire, and it subsequently accelerates the loss of resistance, thus causing premature failure of the structure. Taking into account the spalling risk of concrete, various regulations are often based on experimental approaches, and therefore no predictive calculation can yet be realized. The accurate prediction of this phenomenon remains unknown. In the context of this work, the SAFIRcode may be used to perform a numerical analysis of the spalling risk, by removing layers of concrete covering when a set of spalling criteria are checked. The parametric study focused on: The generalization of the spalling along the element or not, taking account of spalling which occurs on one or more sides of the element, and the influence of various parameters such as changes in boundary conditions and reduced mechanical properties of materials as a function of changes in temperature. The results obtained show the major influence of spalling on the mechanical stability of structural elements in a fire situation, and that this is by reducing the failure time and/or by reducing the yield strength and tangent modulus.

1. Introduction

In the event of fire, structures (buildings, tunnels, etc.) are exposed to high temperatures (up to 1200 °C), causing significant damage, which inevitably leads to deterioration of the surface of the concrete by spalling. The manifestation of this phenomenon was first observed long ago but it is still not well understood in the calculation [1]. This is due to the complexity of the phenomenon. According to several authors [2-4], spalling can be affected by the following factors: the initial strength of the concrete, moisture content, density, the intensity of the fire, the side frame, loading conditions, the type of aggregate, heating rate, the dimensions and shape of the samples. The coupling of these factors can lead to several failure patterns of concrete near the face exposed to the fire.

Moreover, some authors believe that the main causes of the occurrence of this phenomenon are: the low permeability of the concrete, and migration of water vapor into the concrete at elevated temperatures [5-6]. This study focused on the analysis of the failure risk by spalling of a reinforced concrete beam exposed to fire (HC), while assuming that its appearance (spalling) is certain. The study includes two major components, namely:

- Determination of temperature fields in every moment and at every point of the beam, which is done by solving the transient equations of heat transfer using the finite element method. So the beam section is discretized by two-dimensional elements including quadrilateral elements.
- Calculations of the fire resistance with and without consideration of the concrete spalling phenomenon, and the new mechanical properties (tangent modulus, stress and strain) as a function of the thermal field are determined.

2. Mechanisms which lead to spalling

When concrete is subjected to high temperatures, two phenomena can lead to the loss of material: progressive spalling and explosive spalling. From a regulatory point of view, only the explosive spalling term is used (Eurocode 2 [7]; Eurocode 4 [8]). It covers both phenomena, but the term explosive spalling is frequently used in the literature. According to [9-11], spalling of concrete is defined as an aggressive phenomenon which may manifest itself in various less or more violent forms:

Aggregate spalling: Related to the type of aggregate and producing surface damage, this spalling is due to the thermal expansion of the aggregate near the surface, caused by the temperature rise;

Corner separation: This is observed in the lower corners of the concrete and occurs in the later stages of exposure to fire when the concrete has weakened due to the tensile stresses along the edges and corners of the structure where the reinforcement is typically located;

Surface spalling: This type of spalling is characterized by the removal of small pieces flew off the fire exposed surface. Surface spalling may result in exposure of the reinforcement. It is less violent than explosive spalling;

Sloughing off: This type of degradation is due to chemical deterioration of the cement paste, as well as internal cracking of the concrete, caused by the difference in thermal expansion between the aggregate and the cement paste [10];

Post-cooling spalling: This type is a non-violent process with no sound, including complete deterioration of the concrete that may occur weeks after cooling to ambient temperatures, with significant effects on the structural performance [12];

Explosive spalling: violent burst-out of concrete pieces characterized by a sudden release of energy [13]. This phenomenon may occur during the first 30 minutes of fire. It is characterized by large or small pieces of concrete being violently expelled from the surface, accompanied by a loud noise [9]. The explosive spalling of concrete has been observed under laboratory and real fire conditions [12] (Figure. 1).

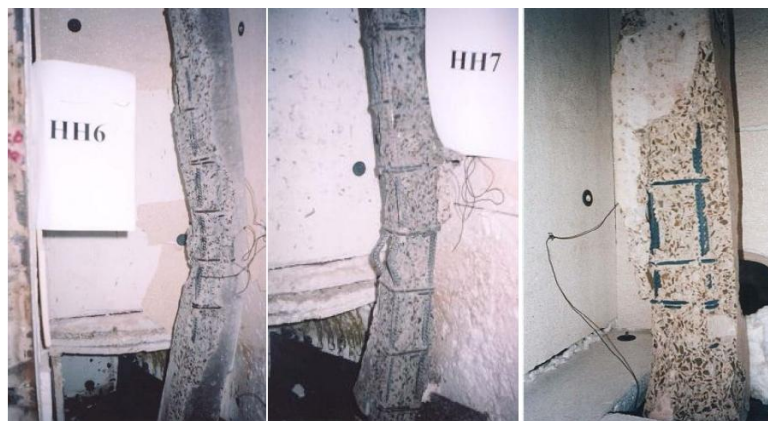


Figure 1: Spalling in HPC columns [14]

3. Process of spalling

The different thermal mechanisms presented above are based on two processes, which are considered to be the main causes of spalling:

3.1. Thermo-hydraulic process

This is associated with the movement of water in liquid and vapor forms. Rapid heat rise in the concrete causes evaporation of free and physically bound water near the concrete surface. This evaporation produces pressure in the pore-network [15]. Some of this evaporated water is evacuated to the heated surface, and the rest migrates to the inside (where the temperature is still low) and is condensed. This creates a quasi-saturated layer that acts as an impermeable wall for gases, resulting in gas pressure build-up (called moisture clog) [16]. In the proximity of this zone the pressure reaches its maximum and thereby produces significant stresses. These cause spalling of the concrete [17]. The state of the rest of the element remains unchanged. Figure 2 illustrates this process.

3.2 Thermo-mechanical process:

This is related to the thermal field in the concrete element [19]. The thermal expansion if prevented generates tensile stress perpendicular to the exposed face [15], thus inducing differential deformations between the cement

paste and aggregates (cement paste contracts, whereas aggregates expand) [16, 20]. This differential thermal behaviour is considered one of the most important causes of degradation of the cement matrix. According to some authors, spalling results from the simultaneous combination of two mechanisms, namely the tensile stresses induced by thermal expansion, and increased interstitial pressure [9, 21-24].

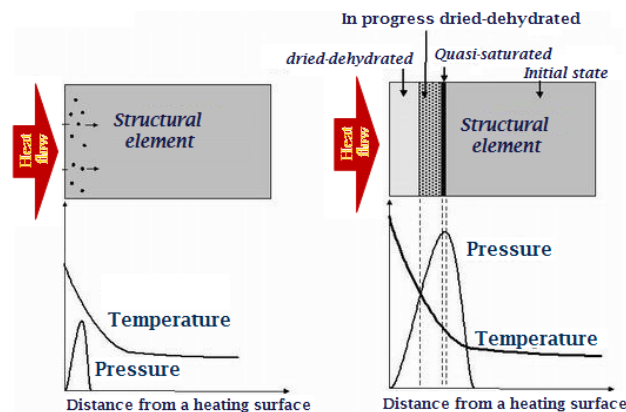


Figure 2: Thermo-hydraulic spalling process [18]

4. Temperature of concrete spalling

Numerous experimental studies have been undertaken to try to understand the phenomenon of concrete spalling and the probability of its occurrence. According to Phan [25], the concrete begins to spall from the first minutes, and when the temperature in the concrete is around 150°C. Khoury and Anderberg [26] concluded that spalling starts within 7 to 20 minutes, when the surface temperature reaches values between 150 and 300 °C. According to Hager [27], the phenomenon may occur at temperatures between 190 and 260 °C. Haniche [28] and Fletcher et al. [29] consider that the spalling phenomenon arises at temperatures between 200 and 350 °C. In other works, it was noted at higher temperatures of the order of 250 – 400 °C [30] and 375 – 425°C [3, 23]. [31] refers to values between 300 and 350 °C. For high performance concrete (HPC), explosive spalling was observed in the temperature range between 300 and 650 °C [32], and between 300 and 350 °C [27]. In this context it should furthermore be added that the rate of temperature increase can be considered as a dominant contributing factor that favors the spalling of concrete. According to Faris [33], a rate of 5 °C/min may be considered sufficient to cause the spalling of concrete.

5. Research context

In order to understand the influence of the spalling risk on the mechanical properties of structures in a fire situation, we have undertaken a numerical modelling of the spalling of a reinforced concrete beam for various boundary conditions: simply supported beam (SSB), propped cantilever beam (PCB) and fixed-fixed beam (FFB). The beam is subjected to the action of the hydrocarbon fire curve (HC) [34] on three sides, with the fourth side having adiabatic conditions. In this context, two situations have been targeted: in the first, the beam is supposed to spall on three sides. In the second situation, it is considered that only the lower face of the beam is affected by spalling. The choice of hydrocarbon fire is because this curve leads rapidly to very high temperatures. We assume that the temperature distribution is uniform over the entire length of the beam, and take account of a global spalling which also occurs in a regular manner along this beam. However, local spalling is assumed to appear at the location where there is the maximum bending moment. For this purpose, the SAFIR software [35] is used, removing a layer of concrete cover (5 mm) whenever the temperature of the exposed surface reaches 400 °C (this temperature seems to be quite sufficient to cause the spalling of concrete) [23, 25, 36], then this process has to be continued up to the total disappearance of the concrete cover. Note that the thickness of the layers removed will be a function of the element thickness used in the finite element analysis. Furthermore, this numerical analysis is divided into two parts: first, the thermal analysis is conducted to determine the temperature distribution in the cross-section of the beam by 2D non-linear transient analysis; secondly, the mechanical analysis is conducted to assess the behaviour of the beam element subjected to elevated temperatures. The characteristics of the materials used in this analysis (steel and concrete) are based on those proposed in the Eurocodes, for concrete according to EC2 2005 and for steel according to Eurocode 3 [37]. The beam is 600 cm long, 30 cm wide and 60 cm high. The following tables present the mechanical characteristics of the materials used.

Table 1: Mechanical characteristics of concrete

Property of concrete (C40/50)		
Compressive strength	f_{c28}	40 MPa
Tensile strength	F_{t28}	0.0
Poisson's ratio	ν	0.2
Type of aggregates		Siliceous
Water content	w	4 %
Cover	C	4 cm
Density of concrete	ρ	2300 kg/m ³

Table 2: Mechanical characteristics of steel

Property of steel ($F_{c,a}500$)		
Modulus of Elasticity	E_a	210 GPa
Tensile strength	F_e	500 MPa
Poisson's ratio	ν	0.3
Reinforcement bare		5HA20

6. Mechanical properties of steel and concrete materials at high temperatures

6.1. Mechanical behaviour of concrete at high temperatures

Figure 3, from Eurocode 4 [8], illustrates the stress–strain relationship model for siliceous concrete under uniaxial compressive stress at elevated temperatures.

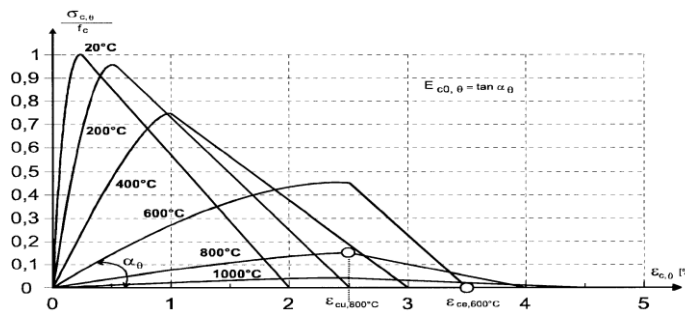


Figure 3: Mechanical properties of siliceous concrete at elevated temperatures [8]

Where f_c : characteristic value of the compressive cylinder strength of concrete at 28 days and at 20°C and $E_{c0,\theta}$: characteristic value for the tangent modulus at the origin of the stress-strain relationship for concrete at elevated temperatures and for short term loading.

This Figure clearly shows the variation of the compressive strength of concrete with the temperature. It can be easily seen that the average temperature of 600 °C in the concrete remarkably reduces the compressive strength to about 50% of its initial value. Figure 4 presents the mathematical model of stress-strain relationship for compressed concrete exposed to high temperature [8].

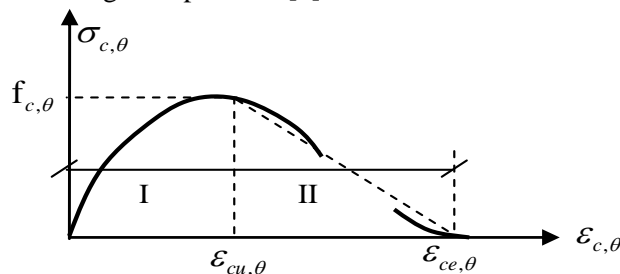


Figure 4: Mathematical model for stress–strain relationship of concrete under compression at elevated temperatures [8]

Where $f_{c,\theta}$: characteristic strength of concrete in the fire situation at temperature θ °C, $\epsilon_{cu,\theta}$: concrete strain corresponding to $f_{c,\theta}$, $\epsilon_{ce,\theta}$: maximum concrete strain in the fire situation $\epsilon_{c,\theta}$: concrete strain in the fire situation,

Range I: In this model, in the strain range from zero to $\varepsilon_{cu,\theta}$, the stress should be determined by applying the following formula (1):

$$\sigma_{c,\theta} = f_{c,\theta} \left[3 \left(\frac{\varepsilon_{c,\theta}}{\varepsilon_{cu,\theta}} \right) / \left\{ 2 + \left(\frac{\varepsilon_{c,\theta}}{\varepsilon_{cu,\theta}} \right)^3 \right\} \right] \quad (1)$$

Range II: For numerical purposes, a descending branch should be adopted.

Another property that influences fire resistance is the modulus of elasticity of the concrete which is greatly reduced at elevated temperature. According to Kodur [38], this large reduction of the elasticity modulus is attributed to the disintegration of hydrated cement products and the breakage of bonds in the microstructure of the cement paste.

Note that the SAFIR software takes into account a transient creep strain within the constitutive relationships for concrete at high temperatures [39]. However, in the Eurocode 2 [7] uniaxial concrete material model, transient creep is included implicitly. But the results are very close using the model that takes into account the implicit transient creep.

6.2. Stress-strain relationship of steel at elevated temperatures

In a similar manner, the strength and deformation properties of steel at high temperature can be determined from the stress–strain relationship shown in figure 5 [8].

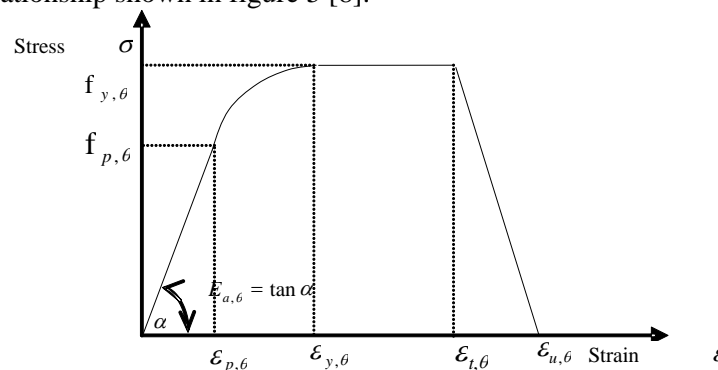


Figure 5: Mathematical model for stress–strain relationships of structural steel at elevated temperatures [8]

where $f_{y,\theta}$: effective yield strength, $f_{p,\theta}$: proportional limit, $E_{a,\theta}$: characteristic value for the slope of the linear elastic range, $\varepsilon_{u,\theta}$: ultimate strain, $\varepsilon_{y,\theta}$: plastic strain, $\varepsilon_{t,\theta}$: yield strain, $\varepsilon_{p,\theta}$: strain at the proportional limit.

The high temperature due to the thermal action of fire has a direct bearing on the main mechanical characteristics of the steel, which determine the conduct of the capacity building elements, such as: yield strength f_y and Young's modulus E . The following Figure 6, from Eurocode 3 [37], shows the considerable influence of high temperature on the mechanical properties of carbon steel.

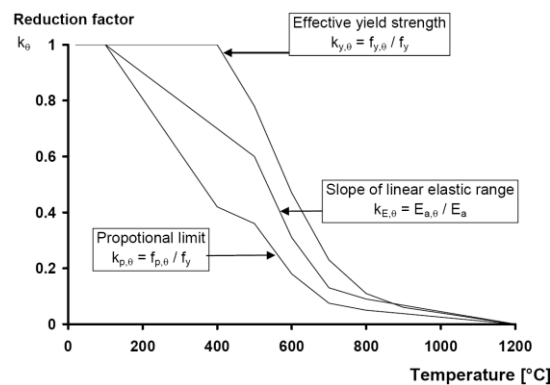


Figure 6: Reduction in mechanical properties of structural steel at elevated temperatures [37]

Where $k_{y,\theta}$: effective yield strength, relative to yield strength at 20 °C: $k_{y,\theta} = f_{y,\theta} / f_y$, $k_{p,\theta}$: proportional limit, relative to yield strength at 20 °C: $k_{p,\theta} = f_{p,\theta} / f_y$, $k_{E,\theta}$: slope of linear elastic range, relative to slope at 20 °C: $k_{E,\theta} = E_{a,\theta} / E_a$

We can see that the steel begins to soften at about 200 °C and begins to weaken at about 400 °C. When the temperature reaches 500 °C, the steel's ultimate strength reduces by 50%. In particular, a steel structure exposed to fire without protection can collapse after 10 – 20 min [40].

7. Fire Models

Several models of time–temperature relationships are available for analysis of the structures in a fire situation, such as the ISO 834 curve [34], ASTM-E119 curve [41], external fire curve [42], parametric fire curves [42], and hydrocarbon curve [42].

For this modelling, we assumed that the beam is subjected to the action of the hydrocarbon fire curve (HC). This curve has a very rapid rise in temperature, reaching a temperature of 900 °C in the first 5 minutes, and held at 1100 °C. According to Eurocode 1 [34], the temperature–time curve of the hydrocarbon fire is given by:

$$\theta_g = 20 + 1080(1 - 0.325 \cdot e^{-0.167t} - 0.675 \cdot e^{-2.5t}) \quad (1)$$

Where θ_g is the gas temperature in the fire compartment (°C), t is the time (min).

8. Thermal analysis

8.1. Modelling of the heat exchangers

According to Franssen [43], the differential equation governing the heat conduction in an isotropic solid material that is incompressible and without mechanical dissipation in Cartesian coordinates, is given by the following equation:

$$\frac{\partial}{\partial x} \left(\lambda \frac{\partial T}{\partial x} \right) + \frac{\partial}{\partial y} \left(\lambda \frac{\partial T}{\partial y} \right) + \frac{\partial}{\partial z} \left(\lambda \frac{\partial T}{\partial z} \right) + Q = c\rho \frac{\partial T}{\partial t} \quad (2)$$

where:

T: temperature, λ : thermal conductivity, ρ : specific mass, c : specific heat, t : time and x, y, z : spatial coordinates. This heat transfer expression is based on the equation of Fourier's Law which was chosen for the SAFIR Software [35].

8.2. Thermal analysis results

The beam is 600 mm deep, 300 mm wide and 6000 mm long. The concrete strength f_{c28} is assumed to be 40 MPa. The beam is reinforced with five 20 mm steel bars of yield strength, $f_y = 500 \text{ MPa}$. The cover depth is assumed to be 40 mm. Temperature dependant material properties for both the concrete and reinforcing steel are taken from Eurocodes. The following figure 7 shows the cross sectional details of the beam.

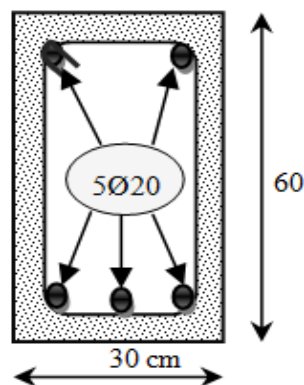


Figure 7: Beams cross section details

As part of this work, the symmetry with respect to the y -axis, and only half of the transversal beam's cross-section with a structured quadrilateral element mesh were considered (figure 8b). The temperature evolution with time at the concrete surface (without spalling) is shown in figure 8a. from this figure, it appears that the two curves (SAFIR software curve and the hydrocarbon curve (HC)) are nearly coincident. This result attests to the performance of the numerical simulation.

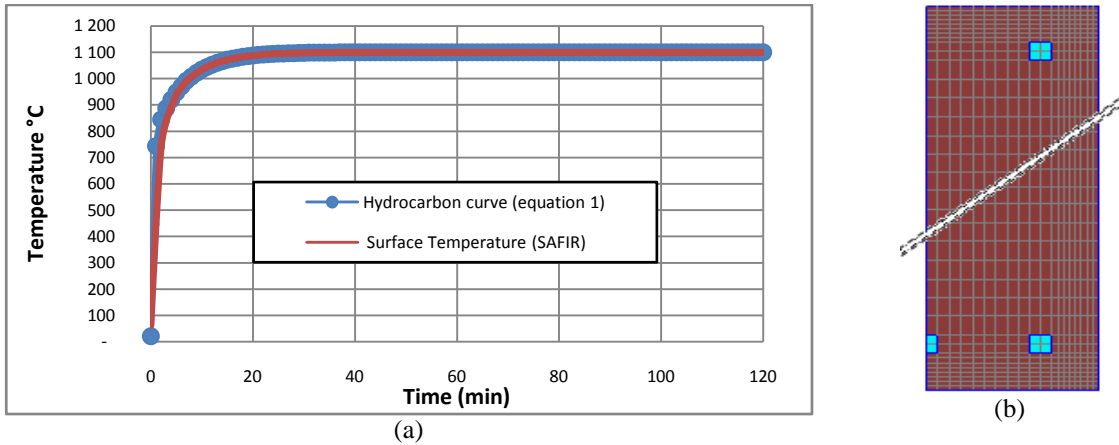


Figure 8: (a) Temperature on the concrete surface obtained by SAFIR and that obtained by the hydrocarbon curve (HC), (b) Discretization of half of the cross-section

Figure 9 illustrates the evolution of the temperature in the section of the beam that is exposed to fire on three sides (accessible). This distribution of flows shows a decreasing temperature towards the centre of the section.

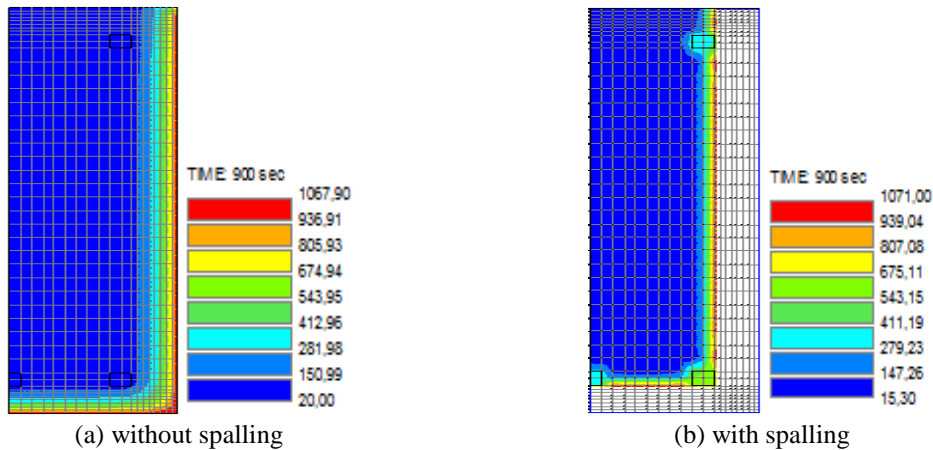


Figure 9: Temperature distribution inside cross-section at 15 min

As shown in figure 9b above, the removal of surface layers of concrete by spalling causes a rapid rise in temperature, exposing the reinforcement nearest the front face to direct flame. Consequently, the concrete cover of the non-spalled cross-section (Figure 9a) slows the heat transfer to the unexposed face of the cross-section. This gives it better resistance. Around the reinforcement, a local disturbance of the heat flow is observed in the concrete, which can be attributed to the thermal conductivity of steel being much greater than that of concrete. In figure 10 below, we present the temperature evolution inside the cross-section of the spall beam. The temperatures are recorded at different depths over time from the exposed surface to the centre of the beam's cross-section. For this purpose, three points have been targeted and their representative curves are shown below: The choice of these points is:

- ✓ Node 460 on the surface of the section,
- ✓ Node 452 at the spalling face,
- ✓ Node 441 in the centre of the section.

From this figure, it is clear that the temperature decreases with distance from the exposed surface to the centre of the beam. After 15 minutes, node 452 reaches a temperature of 1000 °C while core node 441 reaches only 245 °C after two hours of hydrocarbon fire HC exposure. That is, for a thickness of 15 cm (node 441 - node 460), the temperature difference is the order of 850 °C. This shows that the concrete has a good thermal insulation property. In addition, the detachment of the concrete cover accelerates the heat transfer and produces a considerable increase in the temperature. This is explained by the concordance that we clearly observed between the two curves (node 452 and node 460).

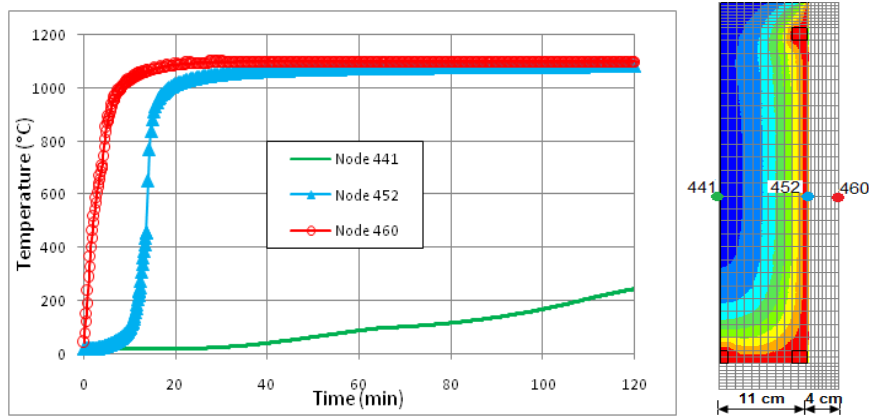


Figure 10: Temperature evolution at different depths within the beam's cross-section spalled on three sides

Similarly, in the following figure we present the temperature evolution of the same nodes of the cross-section for a non-spalled beam.

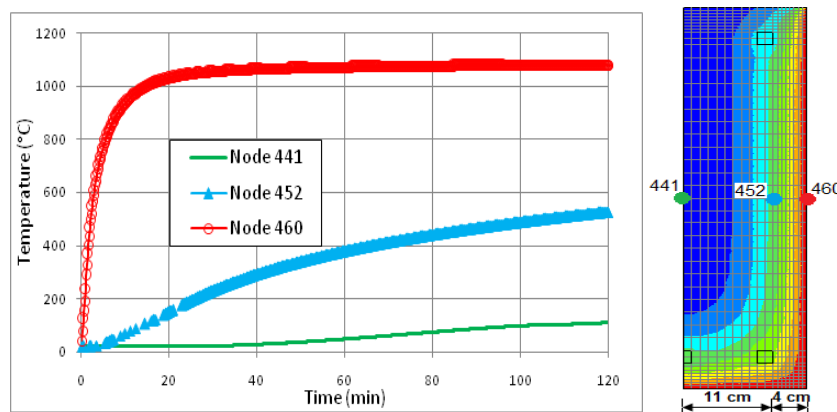


Figure 11: Temperature evolution at different depths within the beam's cross-section (without spalling)

In this case, the node 452 has a slow rise in temperature compared to that recorded for the spalled section (figure. 10). This evolution is concretized by the slight slope with the progression of time, with a heating rate of about 5 °C/min. On the other hand, node 441, which represents the position of the section centre, only reaches a temperature of 106 °C after 120 minutes of fire exposure. Accordingly, the concrete, which transmits heat flow only faintly, will have its centre temperature much lower than the external temperature.

Figure 12 below shows the temperature evolution in the reinforcement corner most exposed to fire (with and without consideration of the spalling phenomenon). There is a strong evolution of the temperature in the steel concrete with spalling (blue curve), which reaches 1100 °C after 30 minutes. At this temperature, all the properties of the two materials (strength and stiffness) become practically nil. This significant increase is mainly due to the detachment of the concrete covering, exposing the reinforcement steel directly to the flame source.

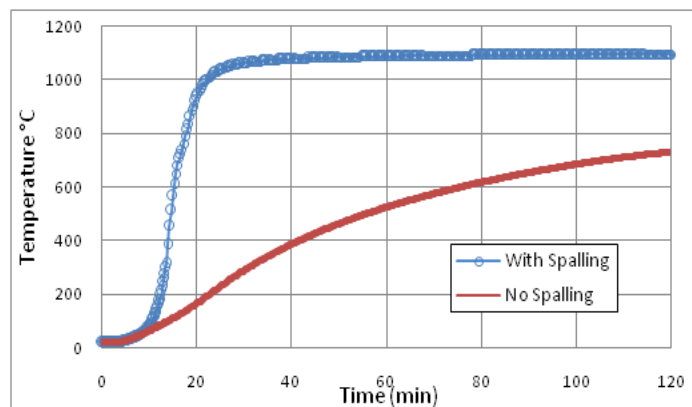


Figure 12: Temperature evolution in steel

9. Structural Analysis

In this study, the beam is longitudinally discretized by Bernoulli type beam elements. The transversal cross-sections of the beam elements are divided into fibers corresponding to those defined in the thermal analysis (The detailed geometry and material properties of the beam are given in section 8.2) .

The beam is subjected to a uniform distributed load of 40 kN/m and is discretized in 21 nodes and 10 elements, as shown in the following figure.

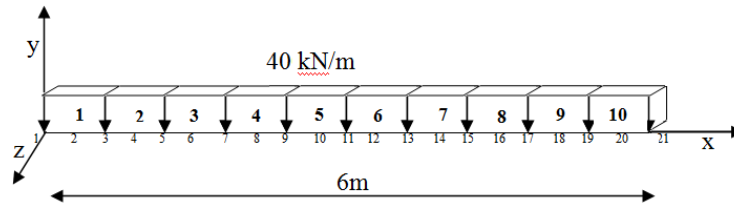


Figure 13: Schematic of the considered beam

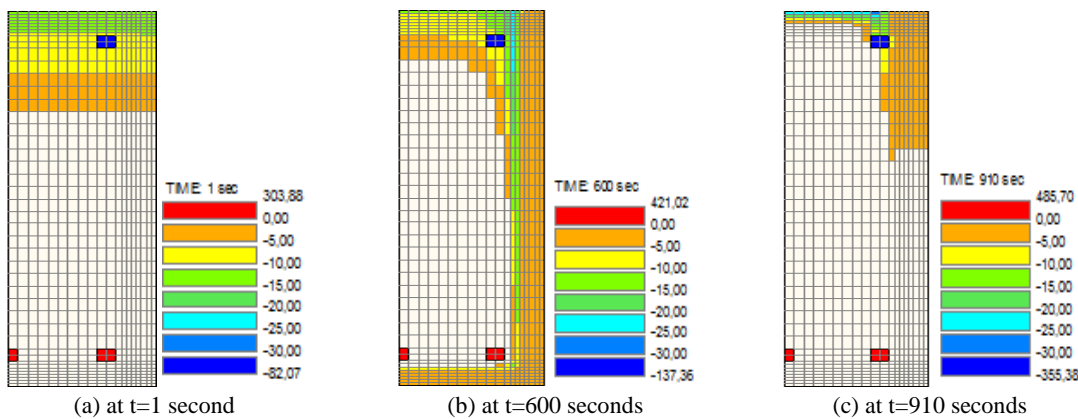


Figure 14: Distribution of thermo-mechanical stress as a function of time

Figure 14 highlights the distribution of thermomechanical stresses in the beam's cross-section as a function of time. The compressed portion which is located on the unheated side has a uniform stress distribution. With time, when the temperature increases rapidly, the temperature gradient which develops in the heated section may damage the material. This damage is due to the high stresses induced by the temperature difference between the heated surface and the core of the beam section. Then the stress distribution at any section is no longer uniform.

Despite the high thermal conductivity of the steel, allowing it to absorb heat much more rapidly than other materials, we see from figure 15 that it loses its initial strength after 15 min of exposure to HC fire, and when the cover layer has completely disappeared (red curve spalled section). Therefore, the concrete cover of the non-spalled section has a retarding effect on the decrease of the thermal conductivity of steel, giving it better resistance (blue curve). This shows that the modulus of elasticity is the most sensitive to elevated temperature when it is exposed directly to the fire source, followed by flexural strength and compressive strength.

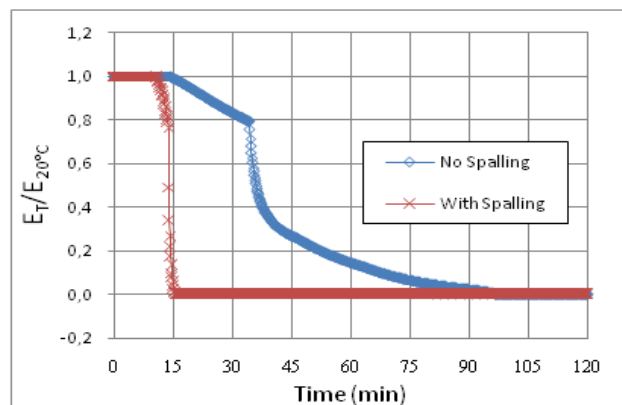


Figure 15: Reduction of the steel elasticity modulus versus time

where:

$E_{20^{\circ}C}$: steel elasticity modulus at room temperature,

E_T : steel elasticity modulus at (t) time (exposed to fire)

Using the exposure to the HC fire curve, the behaviour of the same beams spalled on three sides was compared to those spalled on the one side. We present below the results of structural analysis for different types of beams.

9.1 Beam spalled on three sides

9.1.1. Simply supported beam (with pin-roller supports)

At the left support (pin), the beam is restrained both axially and vertically, while at the right support (roller), it is free to move axially. Figure 16 shows the bending moment of the beam (see figure 16), in the case of a global spalling that occurs along the beam (Figure 16b) and a local spalling that appears in the middle, i.e. at the location of the maximum positive bending moment (elements 5 and 6 in figure 16a).

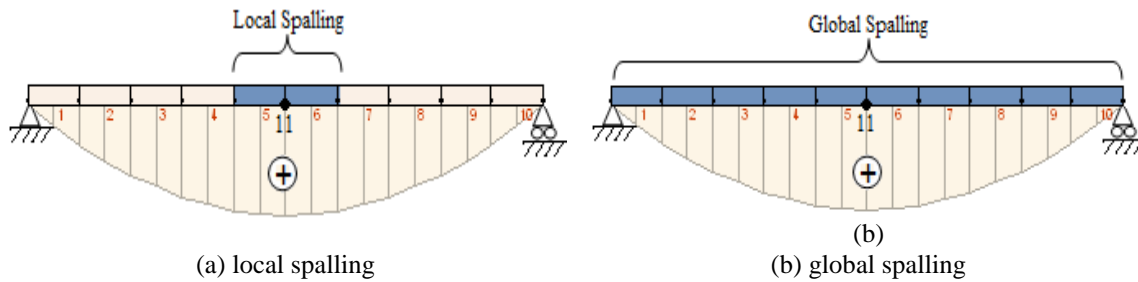


Figure 16: Bending moment diagram with spalled area

In Figure 17, the mid-span deflections of the beams with the two different types of spalling are plotted, showing the comparison between the local and global spalling.

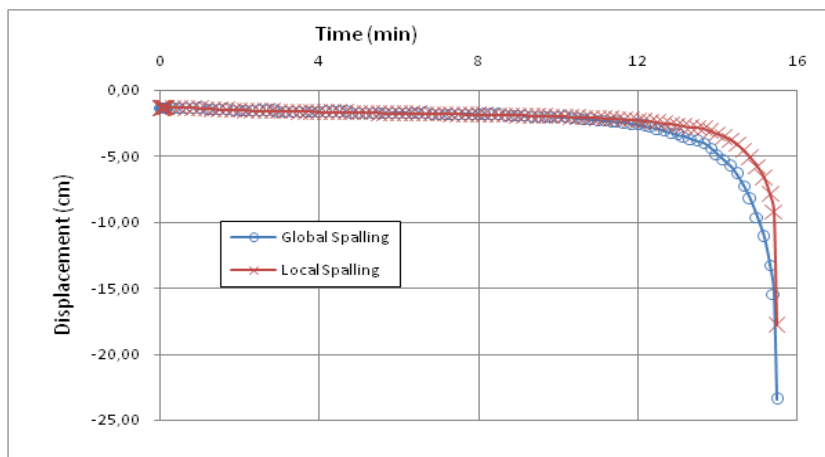


Figure 17: Transverse displacements at mid-span of beam

When the simply supported beam is exposed to fire, it will expand outwards and gradually deflect downwards. The expansion is due to the thermal elongation of the materials. The appearance of spalling at the bottom and on the sides of the beam causes the tensile reinforcement to lose its flexural stiffness, as well as the concrete in the compression zone to lose significantly its compressive strength. This loss of strength and stiffness leads to an increase of the vertical deflection. The shape of this deflection is linear until 14 minutes, then a plastic hinge starts to form in the mid-span and the deflection increases rapidly afterwards. For global spalling, this deflection is about 23.40 cm with a failure time of 15 minutes and 30 seconds. In the case of local spalling, this deflection is of the order of 17.80 cm, corresponding to a failure time of 15 minutes and 30 seconds. However, the non-spalled beam has a very big resistance time which exceeds 99.17 minutes, but it undergoes significant deflection of 29.40 cm (see table 3).

According to this simulation, it is clear that the results are almost identical for both spalling types, which seems logical, because in a statically determinate system, the formation of one plastic hinge is sufficient to cause the collapse of the structure; it is developed at mid-span of the beam (node 11). However, the bending moment along the beam was only due to the imposed load and there was no axial force induced. Furthermore, the moment distribution was constant throughout the heating, as shown in figure 16. There was zero moment at the ends as the beam was free to rotate at its supports, and $qL^2/8$ at the mid-span.

9.1.2. Propped Cantilever Beam with fix-roller supports (PCB)

For this case, the first support of the beam is fixed to move, vertically, axially and rotationally, while the other support (roller) is free to move axially. According to the bending moment diagram (figure. 18), the critical sections exposed to fire and the most affected by the maximum positive bending moment are at the span ($x=5l/8$). We consider the most unfavorable case, and we assume that the local spalling occurs at the (6 and 7) elements of the beam above.

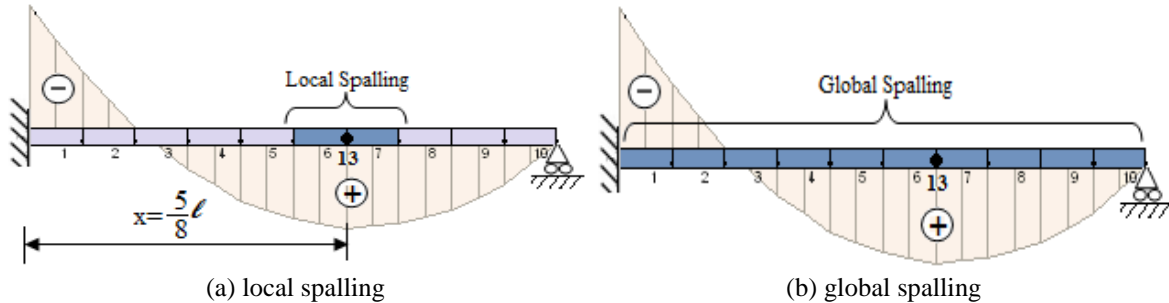


Figure 18: Bending moment diagram with spalled area

Figure 19 illustrates the evaluation of the transverse displacement at mid-span.

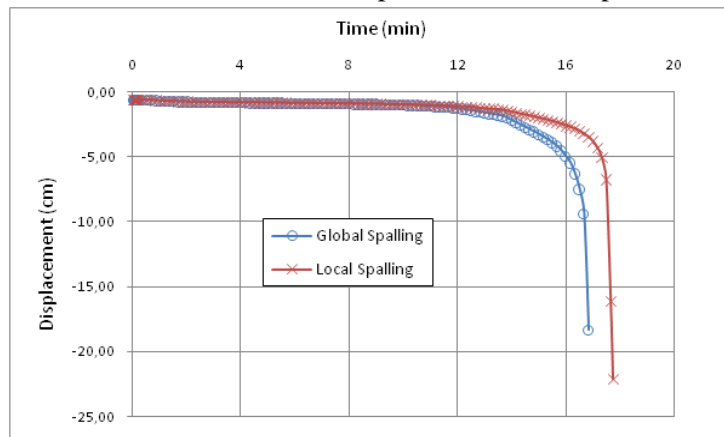


Figure 19: Displacement–time at mid-span

Note that the maximum displacement for local spalling is about 22.11 cm, corresponding to a failure time of 17 min 45 sec, whereas the global spalling causes the failure of the beam in 16 min and 50 sec with a maximum displacement of 18.30 cm.

In view of the results obtained, we can see a relative evolution of the fire resistance of the beam (2 min 15 seconds). This is mainly due to the change in the support system (Adding an embedment changed the failure mechanism i.e. increasing the fire resistance of structure). Bernhart [46] suggests that when a heated member is restrained from thermal expansion by a more rigid surrounding structure, compressive axial forces develop in the beam.

9.1.3. Fixed-Fixed Beam

With fixed supports at both ends, the whole beam is fully restrained, axially, vertically and rotationally. There is negative bending moment induced at the supports, as shown in figure 20. For this case, we have considered a local spalling assumed to appear at mid-span of the beam at elements 5 and 6, where the bending moment maximum of the exposed face is located). The results of the transverse displacements of this simulation are shown in figure 21.

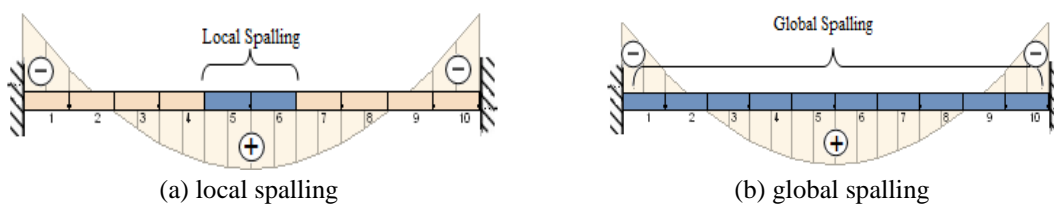


Figure 20: Bending moment diagrams with spalled area

The differential temperature caused a change in the bending moments and thermal expansion caused the development of a compressive axial force. When the applied bending moment exceeds the residual strength of the beam, a plastic hinge will form and failure will occur.

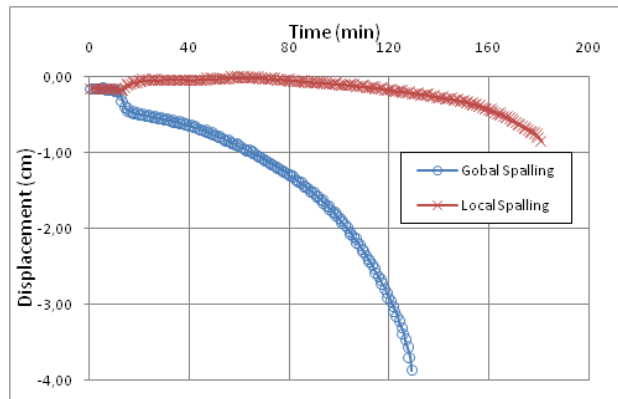


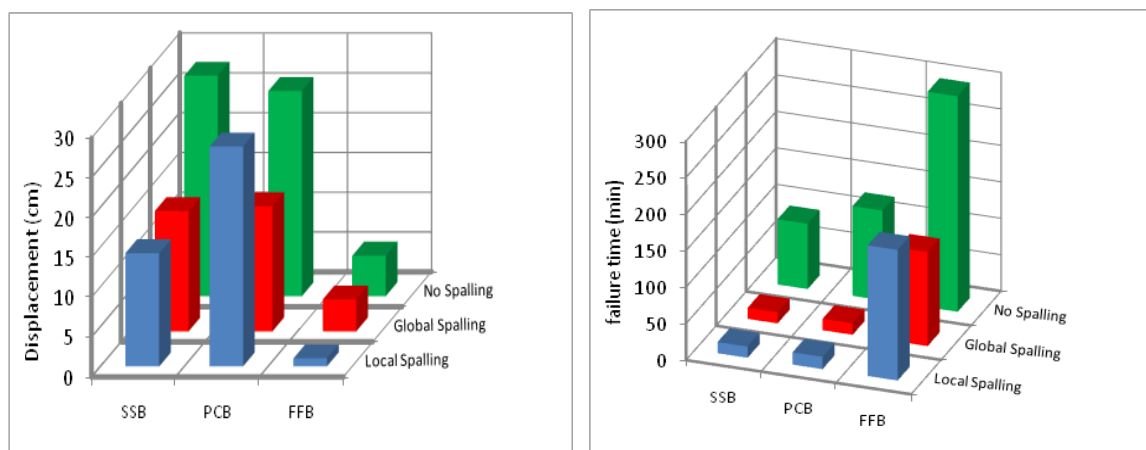
Figure 21: Mid-span deflection of beam

Careful analysis of these curves allowed us to clearly identify the strong evolution of the fire resistance of the beam. We recorded a failure time of 180 min and 55 seconds for local spalling, corresponding to a displacement of 0.9 cm, as against the global spalling which caused a displacement of 3.90 cm for a failure time of 129 min and 20 seconds. According to Linus et al. [47], this best performance in fires is due to moment redistribution which allows the loads to be resisted by alternative means after the first plastic hinge forms. This shows the considerable influence of the degree of embedment on the mechanical behaviour of structures under the effect of thermal actions. The results of this simulation are summarized in the following table.

Table 3: Transverse displacement as a function of failure time for different types of beam

Scenario		Simply supported beam (SSB)	Propped cantilever beam (PCB)	Fixed-fixed beam (FFB)
Local spalling	Displacement (cm)	17.80	22.11	00.90
	Failure time (min)	15.50	17.75	180.92
Global spalling	Displacement (cm)	23.40	18.30	03.90
	Failure time (min)	15.50	16.83	129.33
No spalling	Displacement (cm)	29.40	29.80	5.10
	Failure time (min)	99.17	152.50	302.00

The following histograms illustrate graphically the results of this table.



(a) Comparison of the transverse displacements

(b) Comparison of the failure time

Figure 22: Comparison of the transverse displacements and failure time of the different types of beams

9.2. Beam spalled on one side

Similarly, we present below the results of the transverse displacements and the failure time corresponding to each scenario and according to different boundary conditions:

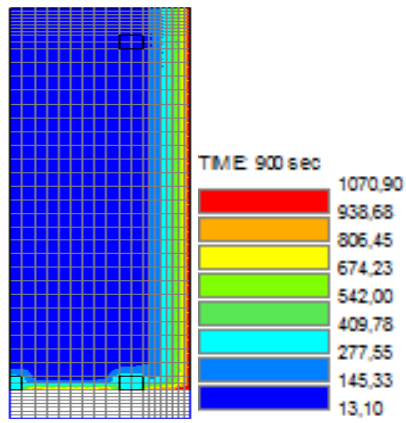


Figure 23: Temperature evolution in the spalled cross-section at $t=15$ min

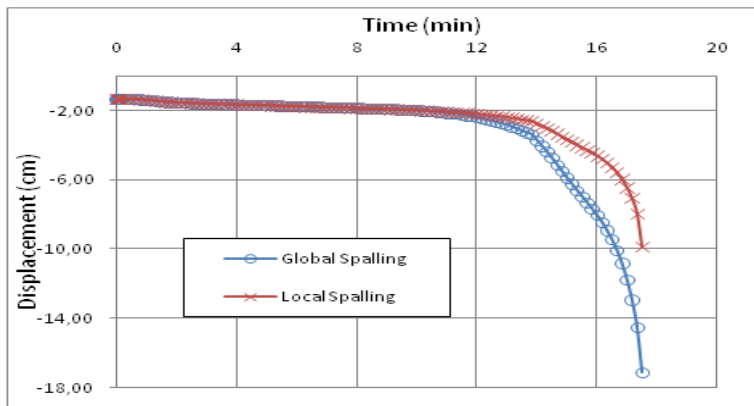


Figure 24: Transverse displacements at mid-span of beam (simply supported beam SSB)

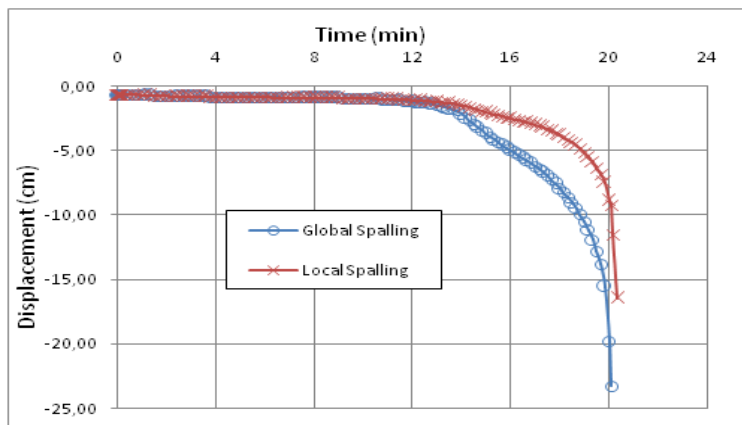


Figure 25: Displacement–failure time of node 13 (propped cantilever beam PCB)

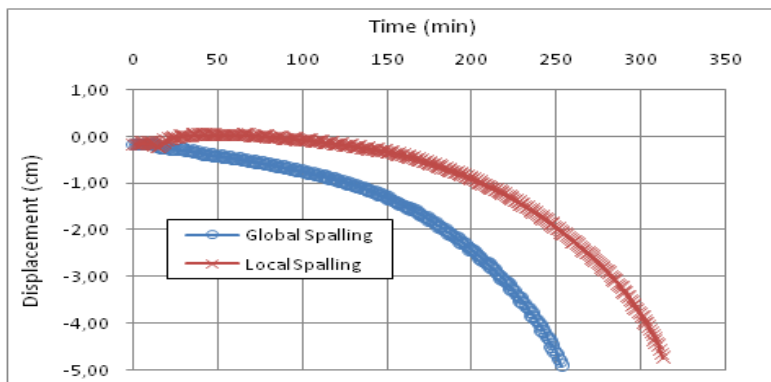


Figure 26: Transverse displacements at mid-span of beam (fixed-fixed beam FFB)

The following table summarizes the results of this simulation.

Table 4: Comparison of failure times (minutes) for various conditions

Scenario		Simply supported beam (SSB)	Propped cantilever beam (PCB)	Fixed-fixed beam (FFB)
Local spalling	Displacement (cm)	09.90	16.50	04.90
	Failure time (min)	17.50	20.33	287.50
Global spalling	Displacement (cm)	17.20	23.30	05.10
	Failure time (min)	17.50	20.08	254.08
No spalling	Displacement (cm)	29.40	29.80	05.10
	Failure time (min)	99.17	152.50	302.00

Figure 27 shows the development of the bending moment at the mid-span (the location of the maximum positive bending moment) for the fixed-fixed beams.

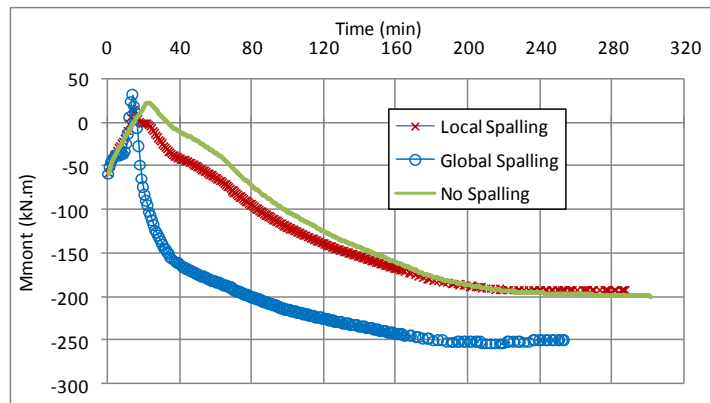


Figure 27: Mid-span moment of fixed-fixed beams (FFB)

During the fire, and when the temperature is increased, the moment resisting supports will steadily increase, which can lead the positive moment at mid-span to change its sign (This change of bending moment sign is due to the thermal load, which acts in the opposite direction of the mechanical load). The value of the bending moment at mid-span is about 31.72 kN.m for global spalling and in the order of 16.57 kN.m for local spalling. However, this value reached 23.09 kN.m for the non-spalled beam. This resistance can reach 302 minutes for local spalling and can exceed 254 minutes for global spalling. It is clear that the fully restrained supports enhance significantly the resistance of structures against spalling. The results above for the beam with spalling on one side reaffirm the crucial role of the support conditions on the structure's behaviour in a fire situation. The direct consequence is that, as with static loads, the hyperstaticity system provides a considerable surplus of structural strength against fire.

10. Volume of concrete spalled

The following table provides information about the percent of total volume of spalled concrete of the beams discussed above.

Table 5: Total volume of spalled concrete

Scenario	Beam spalled on three faces	Beam spalled on one face
Local spalling	6.67 %	01.33 %
Global spalling	33.00 %	06.67%
No spalling	////	////

If spalling occurs along the beam and for the three exposed sides, the total volume of detached concrete resulting from this phenomenon can reach 33% of the total volume of the beam (i.e. a reduction of 33% of the resisting section). This important value effectively constitutes a genuine threat to the stability of the structure, and can also lead to its premature failure.

11. Discussion

When the temperature increases, the concrete begins spalling progressively until the total disappearance of the coating layer, which leads to the reduction in the resisting section of the concrete by 33%. At this time the bearing capacity of the element is weakened under the action of excessive thermal stresses and becomes equal to or lower than the applied stress. After that, a plastic hinge (mechanism) is then formed in the most stressed section. For an isostatic beam, just a single plastic hinge is sufficient for the system to become deformable, and to ruin the beam. However, for a statically indeterminate system, several plastic hinges must be formed before the system becomes deformable.

For the fixed-fixed beam, the ends are blocked by embedding which prevents their axial displacement, the deflection is reduced relative to that which would occur in the case of free support, and stability is greatly increased. This is the case, for example, for a beam of a multiple frame, where the rigidity of the columns situated on either side opposes this displacement.

Conclusion

Until now, no existing model has been able to accurately predict the spalling risk, while its prediction during heating has been largely based on experimental approaches [46]. For the example discussed in this article, we considered that the beam is subjected to the action of a hydrocarbon fire (HC) on three sides. This choice is justified by the fact that the probability of the occurrence and severity of spalling is higher if the heating is applied to several faces than on just one face of the structure [26].

For this purpose two situations were analyzed:

In a first situation, we chose the most unfavorable case; i.e. we assumed that spalling occurs along the beam and on the three sides that are heated, while this is obviously not always the case, because concrete spalling usually occurs in the most exposed locations with elevated temperatures and the most affected by the maximum bending moment. This brings us to the second situation, to consider a local spalling, which is supposed to appear at the location where there is the maximum bending moment.

The following major conclusions can be drawn from the study:

- The failure time by spalling is significantly lower at the tripping time of the cooling phase in the natural or parametric fire (Appendix A Eurocode 1 [34]).
- Compared to the isostatic system, the hyperstatic system has considerable structural performance when subjected to fire.
- The total disappearance of the concrete cover was recorded at a time of 13 minutes while the rupture occurred at 15 minutes and 10 seconds, in other words, immediately after the detachment of the final layer of concrete covering.
- To limit the temperature on the steel reinforcements and avoid concrete spalling, it is recommended to provide a sufficient thickness of concrete covering or to protect the latter by an insulating material.
- For the spalling case, the ejection of the concrete in spall forms on the concrete surface could, in addition to causing a serious reduction in the resistant cross-section of the structural elements, expose the steel reinforcement nearest the front face to high temperatures that can reach 700 °C after 12 min, a temperature at which the steel has no more than 23% of its initial strength (Eurocode 2 [7]) (reduction in the stress and tangent modulus), which leads to a sudden collapse of the structure. Furthermore, the non-spalled concrete, given its low thermal conductivity which gives it good insulating capacity, is able to significantly delay the rise in temperature, thereby protecting the steel reinforcement against excessive temperature and thus an early loss of structural resistance.
- Spalling accelerates the formation of plastic hinges, because the resistant cross-section is weakened by the detachment of the concrete covering.
- For the embedded elements, and in the case where spalling is considered to occur only on one side, the mechanical behaviour of the beam is only slightly affected.
- It is interesting to note that the failure mechanism of the three types of beam with various boundary conditions is the same as for static calculation. Therefore the failure time is considerably affected by spalling.
- In this study, the rotationally restrained beam at the supports reduces the maximum transverse displacement significantly when exposed to a fire. This confirms the results obtained in other work [44, 45].
- The restrained supports enhance significantly the resistance of structures against spalling.

References

1. Kodur, V.R. , *J. F. Prot. Eng.* 15(2), (2005) 93.
2. Dwaikat M.B., Kodur V.K.R., *F. Saf. J.* 44 (2009) 425.
3. Akhtaruzzaman A.A, Sullivan P.J.E, *Imp. coll.of Scien. tech., Conc. Str. Tech., Research report, CSTR 70/2* (1970) 24.
4. Sanjayan G, Stocks L.J., *ACI Mater. J.*, V. 90 (2) (1993) 170.
5. Kodur V.K.R, Phan L.T., *F. Saf. J.* 42 (2007) 482.
6. Phan L.T., *Rep. state-of-the-art. Nat. Inst. Stand. and Tech., Gaithersburg, MD*, (1996) 105.
7. EC2, Eurocode 2., *EN 1992-1-2. Part 1-2.* (2004).
8. EC4, Eurocode 4., *EN 1994-1-2. Part 1-2.* (2004).
9. Khoury G, Majorana C., *Int. Cent. Mech. Scien.* 1(2003).
10. Breunese A.J., Fellingner J. H. H., *Work.-Str. in F.* (2004).
11. Zeiml M., Lackner R., *Proc.: IA-FraMCoS Int. Assoc. of Frac. Mech. Conc. Conc. Str., FraMCoS-6*, (2007).
12. Kodur V.K.R., Dwaikat M. B., *F. Tech.*, 46 (2010) 251.
13. Zeiml M., Lackner R., Herbert A., Mang., *Acta Geot.*, 3(4) (2008)295.
14. Benmarce A.A., Guenfoud M., *Const. and Buil. Mater.*, 57(5) (2005)283.
15. Kalifa P., Menneteau F., Quenard D., *Cem. and Conc. Res.*, 30(12) (2000)1915.
16. Caroline DE. SA., Thèse de Doctorat écol. Nor. Sup. Cachan (2007).
17. LCPC,, Lab. Cent. Pont. Chauss., (2005).
18. www.pentes-tunnels.eu/didactu/tunnel/materiaux/Le%20b%C3%A9ton/Btonsoumisaufeu.html. Retrieved Aug. 15, 2015.
19. Santos S.O., Rodrigues J.P.C., Toledo R., Velasco R.V., “*Act. Polyt., J. Adv. Eng.*, 49(1) (2009)29.
20. NGUYEN V.T., Thèse de Doctorat. Univ. cergy-pontoise, (2013).
21. Geert D.S., *Dam. Conc. Str.*, CRC Press (2012).
22. Franssen J.M., Hanus F., Dotreppe J.C., *Work. f. des. Conc. Str. Mater. Model. Str. Perf.*, (2007)..
23. Deeny S., Stratford T., Dhakal R., Moss P., Buchanan A., *Proc. Inter. Conf. appl. Str. F. Eng.*, (2009)202.
24. Eike W.H.K., *Ph.D. Dissertation, Aachen University* (2014).
25. Minh T.P., *Thèse Doct., Univ. paris-est, France* (2012).
26. Khoury G.A., Anderberg Y., *Rev. Fire saf. desig.* (2000).
27. Izabela G.H., *Thèse Doct., ENPCEP Cracovie.* (2004).
28. Rachid HANICHE., *Thèse Doct., INSA Lyon.* (2011).
29. Fletcher I.A., Welch S., Torero J.L., Carvel R.O., Usmani A., *J. Ther. Scien.* 11(2) (2007) 37.
30. DeMorais M.V.G., Noumowé A., Kanema M., Gallias J.L., Cabrillac R., *24ème Renc. Univ. G.C. (AUGC06), Grande Motte, France* (2006)1.
31. Noumowé A., *Thèse Doct., G. C., Inst. Nat. Scien. Appl., Lyon, France.* (1995).
32. Toumi B., *Thèse de doctorat, Univ. Ment. Constantine, Algérie.* (2013).
33. Faris A., Nadjai A., Silcock G., Abu-Tair A., *F. Saf. J.* 39 (2004)433.
34. EC1, Eurocode 1. ENV 1991-1-2. Part 1-2. (2003).
35. Franssen J.M., *Eng. J., A.I.S.C.*, 42(3) (2005)143.
36. Jeremy J.C., *Thesis Doct., Univ. Canterbury, New Zealand*, (2007).
37. EC3, Eurocode 3. EN 1993-1-2, Part 1-2 (2005).
38. Venkatesh K., *ISRN Civ. Eng.* 2014 (2014)15.
39. Gernay T., Franssen J.M., *F. Sf. J.* 51(2012)1.
40. Victor G., Federico M., *Seis. Desig. Ste. Str., (1st Edition), CRC Press*, (2013).
41. ASTM E119-00, *Stand. Meth. F. T. Buil. Const. Mater., Am. Societ. Test. Mater., West Consh., PA, USA* (2007).
42. EC1, Eurocode 1. ENV 1991-2-2. Part 2-2. (2003).
43. Franssen J.M., *Post doc. thesis, Agrég. Enseig. Supé., Univ. Liège.* (1997).
44. Bernhart D., *Dipl. Thesis, Univ. Karlsruhe, Germany, and Univ. Canterbury, New Zealand* (2004).
45. Linus C. S. Lim., *Doct. thesis of Phil., Univ. Canterbury Christchurch, New Zealand.* (2003).
46. Maraveas, C., Vrakas, Apostolos A., *Str. Eng. Int.* 24(3) (2014) 319.
47. Linus L., Andrew H.B., Peter J.M., *F. Mater.* 28 (2004)95.

(2017) ; <http://www.jmaterenvironsci.com/>